Nonuniversality of front fluctuations for compact colonies of nonmotile bacteria

Silvia N. Santalla,[1] Javier Rodríguez-Laguna,[2] José P. Abad,[3] Irma Marín,[3] María del Mar Espinosa,[4] Javier Muñoz-García,[5] Luis Vázquez,[6] and Rodolfo Cuerno[5]

[1]*Departamento de Física and Grupo Interdisciplinar de Sistemas Complejos (GISC), Universidad Carlos III de Madrid, Leganés, Spain*
[2]*Departamento de Física Fundamental, Universidad Nacional de Educación a Distancia (UNED), Madrid, Spain*
[3]*Departamento de Biología Molecular, Universidad Autónoma de Madrid (UAM), Cantoblanco, Madrid, Spain*
[4]*Hospital Universitario Puerta de Hierro, Madrid, Spain*
[5]*Departamento de Matemáticas & GISC, Universidad Carlos III de Madrid, Leganés, Spain*
[6]*Instituto de Ciencia de Materiales de Madrid (ICMM), Consejo Superior de Investigaciones Cientficas (CSIC), Madrid, Spain*

(Received 14 February 2017; revised manuscript received 19 June 2018; published 10 July 2018)

The front of a compact bacterial colony growing on a Petri dish is a paradigmatic instance of non-equilibrium fluctuations in the celebrated Eden, or Kardar-Parisi-Zhang (KPZ), universality class. While in many experiments the scaling exponents crucially differ from the expected KPZ values, the source of this disagreement has remained poorly understood. We have performed growth experiments with *B. subtilis* 168 and *E. coli* ATCC 25922 under conditions leading to compact colonies in the classically alleged Eden regime, where individual motility is suppressed. Non-KPZ scaling is indeed observed for all accessible times, KPZ asymptotics being ruled out for our experiments due to the monotonic increase of front branching with time. Simulations of an effective model suggest the occurrence of transient nonuniversal scaling due to diffusive morphological instabilities, agreeing with expectations from detailed models of the relevant biological reaction-diffusion processes.

DOI: 10.1103/PhysRevE.98.012407

I. INTRODUCTION

Active matter, i.e., the emergent behavior of a large number of agents that can produce mechanical forces via energy dissipation [1], is recently proving itself as an extremely rich context for non-equilibrium phenomena. Instances range from schools of fish or bird flocks, to vibrated granular rods or propelled nanoscale or colloidal particles, for all of which fluctuations play a conspicuous role in the collective dynamics [2].

Bacterial systems [3] provide further instances of active matter, from microswimmer suspensions in which single cell motility plays a crucial role [4,5] to bacterial colonies, in which motility can be hampered [6–8]. Actually, the fronts of bacterial colonies have long been held as textbook examples [9–11] on how interactions among individuals lead to collective, highly correlated behavior. For experiments frequently done using *Bacillus subtilis* or *Escherichia coli*, this ranges from the formation of characteristic patterns—like diffusion-limited aggregation (DLA) fractals, concentric rings, or dense-branched morphologies—to formation of disks or of compact, but rough, morphologies [7,12–15], all of which are also found in other, non-living, systems.

The simplest situation in which individual bacterial motility is fully suppressed by a high agar concentration on the supporting Petri dish has received particular attention, as it paradigmatically demonstrates a change from DLA branches to compact, Eden-like, clusters, for an increasing nutrient concentration [8,12], akin to that found for many other diffusion-limited (DL) growth systems [16]. This morphological transition has been recently shown to bear direct importance on the biological performance of the colony [17–19]: branches enable the space segregation of cell lines which respond differently with respect to the production of enzymes needed for biofilm formation, enhancing the prevalence of cooperative cells. Biofilms are surface-attached communities hosting most living bacteria in nature, of paramount importance to medicine and technology, from infections to energy harvesting [20,21].

Furthermore, front fluctuations of Eden clusters [22] are in the celebrated Kardar-Parisi-Zhang (KPZ) [23] universality class of kinetic roughening [10,24,25]. Sparked by breakthroughs on exact solutions of the KPZ equation and related growth models, that have been experimentally validated (see [26] for a review), this class is recently being demonstrated as a paradigm for strong fluctuations in one dimension (1D), as found, e.g., in non-linear oscillators [27], stochastic hydrodynamics [28], quantum liquids [29], or reaction-diffusion systems [30]. Remarkably, in the low motility case, most experimental values found for the scaling exponents of compact Eden-like bacterial colonies *do not* coincide with the KPZ values [8,13,14]. This fact has been reconciled with a putative Eden behavior via, e.g., effective quenched disorder [8], unexpectedly for a system which is successfully described by continuum [31–36] or discrete [17,37,38] models with no source of quenched disorder.

In this article, we report colony growth experiments for *B. subtilis* and *E. coli* under suppressed-motility conditions [15,39] in the alleged Eden regime. We explain the non-KPZ kinetic roughening that we indeed observe as nonuniversal scaling behavior induced by the diffusive instabilities that occur. This is achieved by comparing our data with simulations of a continuum model that we formulate, indicating that these experimental conditions keep the system within a DL transient for all accessible times. Moreover, the increase of front branching with time for the experimental colonies prevents

asymptotics from being in the KPZ universality class under our suppressed-motility conditions. Analogous nonuniversal behavior has been identified in other DL systems, like thin film growth by electrodeposition (ECD), by chemical vapor deposition (CVD) [16,40], or in coffee ring formation by evaporating colloidal suspensions [41–44].

The paper is organized as follows. Our experimental setup and methods are described in Sec. II, while a continuum model which we employ to rationalize our observations is described in Sec. III. This is followed by our experimental results, which are reported in Sec. IV. Further discussion is provided in Sec. V, which also contains our conclusions and an outlook on future work. Further technical details on error estimates are left to an appendix.

II. EXPERIMENTAL SETUP

We have grown colonies of *B. subtilis* 168 (BS) and *E. coli* ATCC 25922 (EC) on Petri dishes as in [15,39], in the high agar concentration (i.e., low motility) regime for different concentrations of nutrients. Specifically, we have kept a constant agar concentration $C_a = 10$ g/l while considering different values of the nutrient concentration, $C_n = 10, 15$, or 20 g/l, within the Eden-like region in the morphological space of [15,39]. These conditions correspond to a value for the non-dimensional thickness δ of the active layer within the bacterial colony, where the nutrient concentration has non-negligible gradients [17,33,36–38], which is large enough for the colony to look compact on the accessible space-time scales.

For inoculating Petri dishes, bacteria were grown overnight in nutritive liquid medium [5 g/l NaCl (Merck, Germany), 3 g/l meat extract (Merck, Germany), 10 g/l bacto-peptone (Lab. Conda, Spain)] and the OD600 was measured. Cells were pelleted at 12 krpm in a microcentrifuge, and resuspended to 0.5 OD600 in minimal medium without bacto-peptone. Two replica Petri dishes were prepared following [39]: a 3 mm thick agar plate in nutritive medium [5 g/l NaCl (Merck, Germany), 5 g/l K_2HPO_4 (Carlo Erba, Italy) and bacto-peptone (Lab. Conda, Spain)] inoculated at the center with 1 μl of the cell suspension was incubated at 35°C in a sealed humid chamber for up to 33 days, leading to growth of quasi-2D colonies. No swarming of bacteria has been detected.

Pictures were taken at different incubation times using a digital camera (Olympus SC30, Japan; 3.3 Mp) coupled to a stereo microscope (Olympus SZX10), or a digital camera (Nikon D5000, Japan; 12.3 Mp) for large enough colonies. These photographs were treated to extract the position of the colony front at each growth time, see Fig. 1.

A. Extraction of front profiles

We next consider the protocol that we have followed in order to extract the position of the fronts of the bacterial colonies from the photographs. The analysis was semi-automatic. An algorithm was developed, which works in the majority of the cases without supervision. The images were digitized and subject to a contrast filter in order to highlight the interface. The resulting image can be regarded as a matrix with entries equal to 1 inside the colony and equal to 0 outside the colony. Then, a discretized continuous curve was obtained as follows. First,

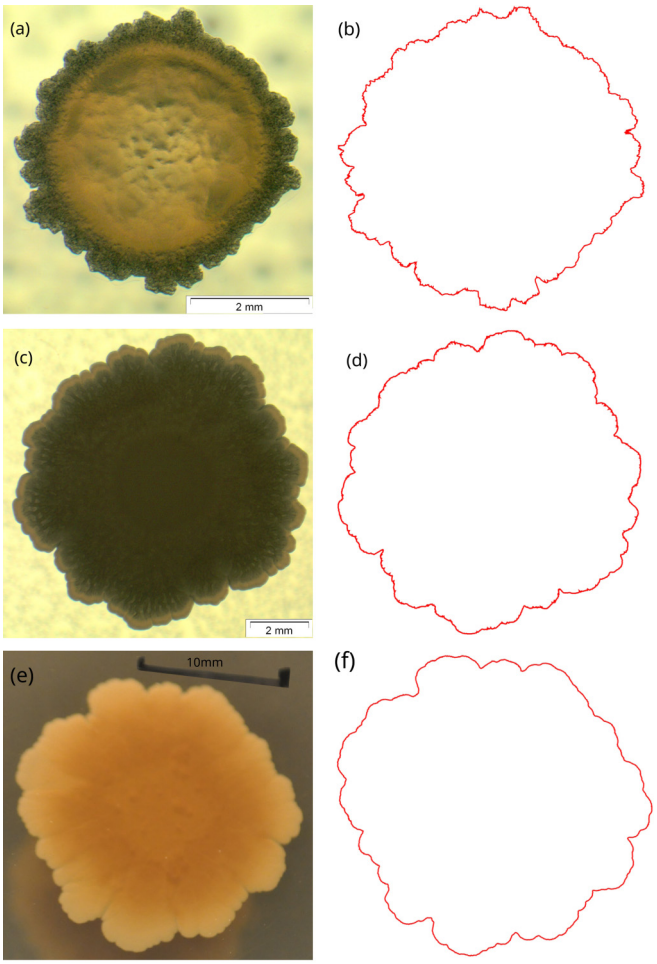

FIG. 1. Experimental photographs of the bacterial colonies [left column, (a, c, e)] and profiles extracted using the procedure described in the text [right column, (b, d, f)]. All these examples corresponds to *B. subtilis* with $C_n = 20$ g/l. The growth times are: (a, b) 19 h, (c, d) 168 h, and (e, f) 792 h, top to bottom.

the geometric center of the colony bulk was estimated. Then we obtained the intensity curve along rays emanating from that point for different angles, $I_\theta(r)$. For each angle θ, we obtained the distance $r(\theta)$ from the center, such that a certain threshold value of the total intensity was found below it. Mathematically,

$$\int_0^{r(\theta)} dr\, I_\theta(r) = \mu \int_0^{\infty} dr\, I_\theta(r), \tag{1}$$

where μ is the threshold parameter. In our present case, $\mu = 0.99$ was employed, i.e., the radius $r(\theta)$ is defined as the first percentile of the intensity distribution. As an illustration, Fig. 1 shows a set of experimental photographs and their corresponding profiles. Note the compact form of the bacterial colony, delimited by a well-defined front that fluctuates around an average circular shape.

III. EFFECTIVE MODEL

The evolution of the colony front can be rationalized through a kinetic continuum model for the dynamics of the front position. In this model the detailed dynamics of relevant

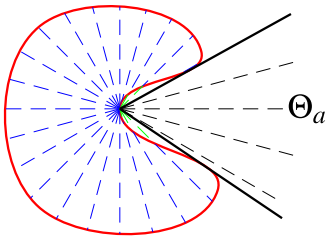

FIG. 2. Given an interface (shown by the curved red solid line), and a point $\vec{r}$ on it, let us consider all the rays emanating from this point (dashed straight lines), and find out the fraction of rays that do not intersect the interface again (those delimited on the right side of the figure by the straight black solid lines). Such a fraction provides the local aperture angle, $\Theta_a(\vec{r})$.

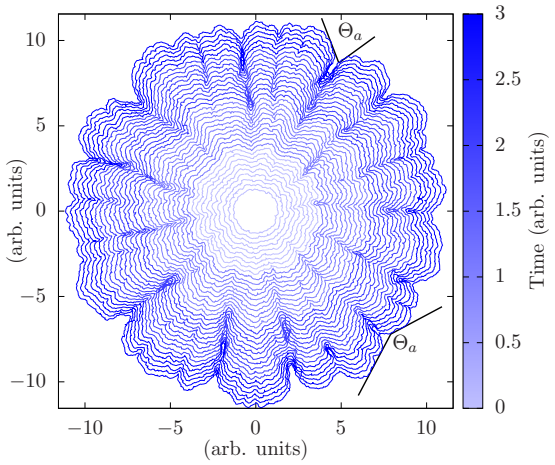

FIG. 3. Interfaces from numerical simulations of Eq. (2) for $A_0 = 0$, $A_1 = 0.1$, $A_a = 1$, $A_n = 0.1$, and a circular initial condition. Sketches further illustrate the meaning of the local aperture angle $\Theta_a(\vec{r})$. The growth time for each profile can be read from the color bar on the right. Space and time units are arbitrary.

physical fields (e.g., bacterial and nutrient densities) other than the position, $\vec{r}(t)$, of the front itself, is neglected. The model is tailored so as to capture purely the form and the dynamics of the front, in a similar way to many other instances of diffusion-limited growth, like thin solid films [45–47] or combustion fronts [48,49], in which this type of approach has proven useful. Specifically, we consider

$$\partial_t \vec{r} = (A_0 + A_1 K(\vec{r}) + A_a \Theta_a(\vec{r}) + A_n \eta)\vec{n}, \qquad (2)$$

where $\vec{r}$ is an interface point, $\vec{n}$ is the local exterior normal, $K(\vec{r})$ denotes the curvature of the interface at that point, $\Theta_a(\vec{r})$ is the local aperture angle, and η is a zero-average Gaussian uncorrelated space-time noise. Furthermore, A_0, A_1, A_a, and A_n are parameters which quantify, respectively, the relative strengths of the average growth velocity of a planar front, surface tension, the dependence on the aperture angle, and fluctuations. Equation (2) is similar to continuum models earlier put forward in the context of growth of thin solid films limited by diffusive transport, see, e.g., [11]. Note that, in contrast with many works in that field, Eq. (2) applies to interfaces with an arbitrary geometry, in particular with an average circular shape, and is not affected by small-slope, nor no-overhang approximations. In this sense, the model can be considered a stochastic generalization of a previous equation put forward in the context of combustion fronts [48,49], for which transport also takes place by diffusion.

In our model, we assume that growth resources increase locally with the angle under which a given point $\vec{r}$ at the interface sees the exterior world, which we describe as the *aperture angle*, $\Theta_a(\vec{r})$, which is illustrated by the sketch in Fig. 2 and further in Fig. 3. Intuitively, points inside cavities get less nutrient than those at local protuberances. As frequently done in the context of diffusion-limited growth, one may make an analogy [11] to an ensemble of grass leaves which are striving to collect sunlight: taller leaves cast shadows on shorter ones, hindering growth of the latter. With this metaphor in mind, we consider this term to implement a *shadowing effect*, as frequently done in the context of DL growth [11]. Mathematically, the computation of the aperture angle is performed as follows. Let Γ be the interface with $\vec{r}_0$ and $\vec{r}$ being points on it. Let $A(\vec{r},\vec{r}_0)$ be the angle under which $\vec{r}$ is seen from $\vec{r}_0$. Then, the aperture angle from point $\vec{r}_0$ is given by

$$\Theta_a(\vec{r}_0) = 2\pi - |\mathrm{Range}_{\vec{r}\in\Gamma}(A(\vec{r},\vec{r}_0))|, \qquad (3)$$

i.e., the measure of the range of function $A(\vec{r},\vec{r}_0)$ when $\vec{r}$ takes values on Γ.

Equation (2) implements the basic mechanisms influencing growth dynamics: on average, the front tends to minimize its length and grows along the local normal direction, faster at those locations $\vec{r}$ which are more exposed [larger aperture angle $\Theta_a(\vec{r})$] to the external diffusive fluxes; moreover, the front position experiences stochastic fluctuations related with microscopic events (nutrient transport and consumption, as well as cell division and relocation). The choice of these mechanisms is supported by more detailed continuum models of bacterial colonies [33,35,36] which find the front to be unconditionally unstable to perturbations. In particular, no quenched disorder is assumed.

In order to simulate Eq. (2), we have proceeded along the lines of [50,51]: the interface is discretized in an adaptive way, adding and removing points dynamically in order to keep a constant spatial resolution. The normal vector and the local curvature are computed using concepts from discrete geometry. An important element of the simulation is that the interface is always a simple curve, although it can have *overhangs*: self-intersections are removed.

The evaluation of the aperture angle is the most costly part of the calculation to simulate Eq. (2), since it is a global measurement. We have devised the following algorithm in order to compute it. Given a point P and a segment P_1P_2, we define the minimal angle-interval as the counterclockwise ordered pair $\alpha(P, P_1P_2) \equiv (\alpha_0,\alpha_1)$ of angles, with respect to the horizontal, under which the segment is viewed from the point. If a segment is extended to a chain $P_1 \cdots P_n$, we just compute the union of all angle intervals. The aperture angle is the complementary of the measure of the final angle interval.

In order to assess the type of morphological instability implied by the aperture term in Eq. (2), we have simulated it numerically by setting to zero all other terms in the equation. We have performed a linear stability analysis of the ensuing model by studying the rate of growth or decay in time for sinusoid-like perturbations of an overall circular shape (not shown). We have verified the expected unstable behavior: the amplitude of a small perturbation grows with a velocity proportional to the wave-number k of the perturbation. In the case of a band geometry with periodic boundary conditions, this means that, according to Eq. (2),

$$\partial_t h_k(t) \simeq |k|\, h_k(t) + \cdots , \tag{4}$$

where $h_k(t)$ is the amplitude of a small sinusoidal perturbation of a flat profile with wave-vector k. This is indeed the well-known behavior of the aperture-angle term, as elucidated in other diffusion-limited systems [11,48,49]. The growth law Eq. (4) corresponds specifically to the destabilizing component of the classic Mullins-Sekerka instability, paradigmatic of diffusion-limited growth [9,11].

Figure 3 shows the time evolution of an initially circular interface described by Eq. (2), as obtained from numerical simulations for a representative choice of parameters. Once the interface perimeter grows large enough, the shadowing instability indeed sets in, reflecting the preferential growth at front protrusions, as compared with front troughs. In strong similarity with the experimental profile on the Fig. 1, the colony remains a compact aggregate for all t, with a front that fluctuates around an average circular shape.

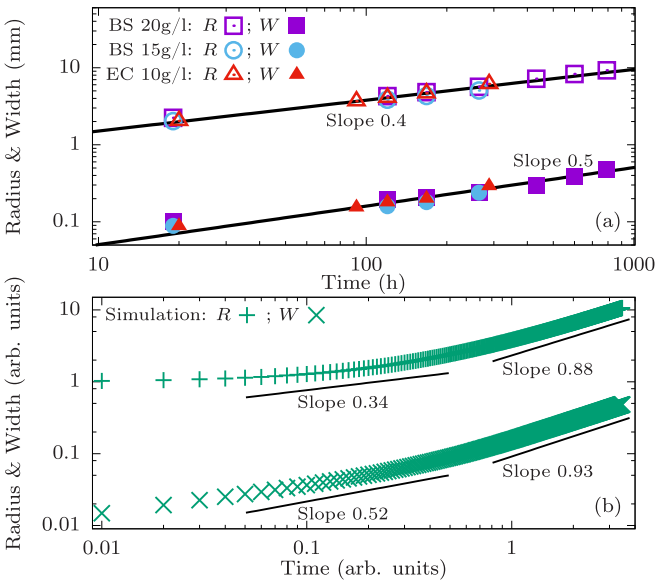

FIG. 4. (a) Experimental radius R (open symbols) and roughness W (solid symbols) vs growth time. Purple and blue (red) symbols are for BS (EC), with C_n as in the legend. Lines are fits to power-laws, $R \sim t^n$ and $W \sim t^\beta$ with $n \approx 0.4$ and $\beta \approx 0.5$. (b) $+$ ($\times$) symbols are data for R (W) from numerical simulations of Eq. (2) for parameters as in Fig. 3, averaged over 500 noise realizations. The lines represent power-laws $R \sim t^n$ and $W \sim t^\beta$ with different values of n and β for short and long times, as indicated. Units are arbitrary.

IV. EXPERIMENTAL RESULTS

In this section we report our experimental results for BS and EC colonies. Along with the various experimental properties studied, we additionally consider numerical simulations of Eq. (2) as aids to interpret the experimental results.

A. Time evolution: Radius and global roughness

We first consider quantitatively the time evolution of our experimental BS and EC colonies through the average radius and global roughness of the colony fronts: After front extraction as described in Sec. II, each profile is a set of N points on the plane, $\{x_i, y_i\}_{i=1}^N$. This set is employed to obtain the radius, R, of the best fitting circle, using a minimization procedure to find the corresponding center (x_C, y_C). The deviations from the fitting circle provide the *global roughness* or surface width,

$$W \equiv \left\langle \frac{1}{N} \sum_{i=1}^{N} \left(\sqrt{(x_i - x_C)^2 + (y_i - y_C)^2} - R\right)^2 \right\rangle^{1/2}, \tag{5}$$

where brackets denote averages over experimental realizations. Both the radius and the global roughness of the experimental colony fronts depend on growth time. Results for $R(t)$ and $W(t)$ are provided in the top panel of Fig. 4. Data can be fit by power laws in both cases, $R(t) \sim t^n$ and $W(t) \sim t^\beta$, with $n \simeq 0.38$–0.43 and $\beta \simeq 0.47$–0.52 values which are similar for different nutrient concentration values and bacterial species. Usually, for experimental circular interfaces that display Eden/KPZ fluctuations [41,52]—conspicuously including (Vero) cell aggregates [53]—the average front velocity is constant, hence the average front position increases linearly with time. At variance with this, the radial growth rate we measure is sublinear, i.e., $n < 1$. On the other hand, W follows power-law behavior with time as in standard kinetic roughening systems. Taking into account that uncorrelated surface growth (so-called random deposition, RD) is characterized by $\beta_{RD} = 0.5$ [10], our relatively large experimental β values are suggestive of uncorrelated, or possibly unstable growth wherein front fluctuations are amplified and grow even faster than in mere RD [9–11]. As noted in [8], to date no other experimental work on bacterial colony growth provides information on the time evolution of $R(t)$ or $W(t)$ under our working conditions, in spite of the fact that universality classes are defined by two independent exponents [9–11], one of them related with time-dependent behavior.

For the sake of comparison, the bottom panel of Fig. 4 shows the average radius and global roughness obtained from numerical simulations of our model, Eq. (2). Apparently in contrast with the experiment, for each magnitude two different regimes can be distinguished, one for short times and a different one for long times, within which the power laws are characterized by different exponent values. Note that the numerical values of the exponents which are closest to those of the experiments correspond to the model short-time regime. Actually, taking, e.g., BS colonies with $C_n = 20$ g/l as a representative case, we can make a more detailed comparison between the experimental behavior of $W(t)$ and $R(t)$ with that predicted by Eq. (2).

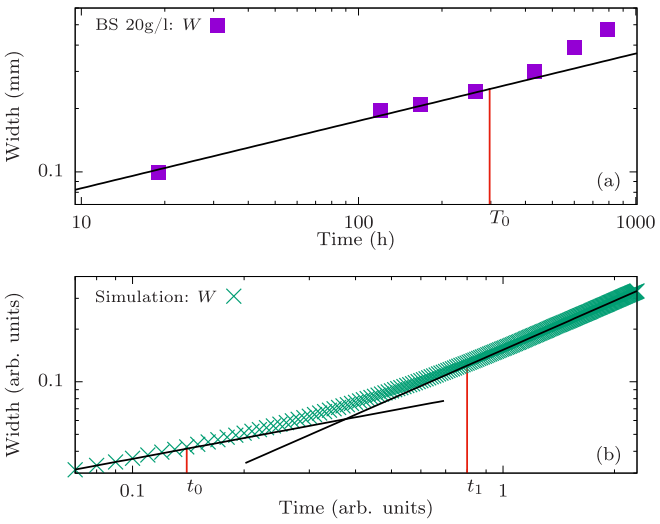

FIG. 5. (a) Magnified view of the global roughness of a BS bacterial colony studied in Fig. 4. The time marked as T_0 indicates a change in the power-law behavior. (b) Magnified view of the roughness from numerical simulations of Eq. (2) using parameters as in Fig. 4. Time t_0 corresponds to the initial change in scaling behavior. Time t_1, signaling the beginning of asymptotic, long-time behavior, is also indicated.

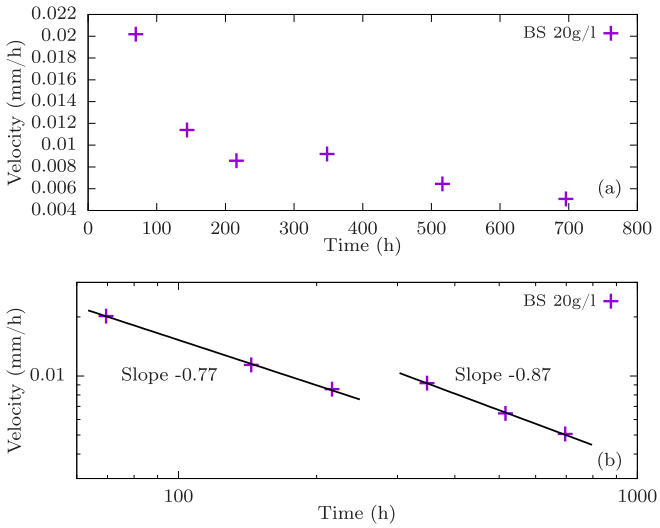

FIG. 6. Average front speed as a function of time for BS experiments using $C_n = 20$ g/l in linear (a) and doubly logarithmic (b) displays. The data group themselves into two scaling regimes, approximately separated at $T_0 = 297$ h.

1. Simulations in physical units

The experimental data for the evolution of the global roughness agree closely with the early time behavior of the simulations; these were performed for several sets of parameter values with very similar results. The specific choice given in Fig. 3 (namely, $A_0 = 0$, $A_1 = 0.1$, $A_a = 1$, and $A_n = 0.1$) turned out to be the most relevant one to our experimental system. Of course, the units for these constants are arbitrary in principle. However, we can convert them into physical units through detailed comparison with the experimental data, as follows.

In Fig. 5(a) we show the roughness of the interface, $W(t)$, for the same *B. subtilis* experiments with $C_n = 20$ g/l considered in Fig. 4, but in a magnified view. A certain time $T_0 = 297$ hour (h) can be identified which marks a change in the power-law behavior of the data, at which the global roughness is $W_0 = 0.25$ mm. The experiment ends at time $T_e = 801$ h, when $W_e = 0.47$ mm. Thus, we have $W_e/W_0 = 1.9$ and $T_e/T_0 = 2.7$. The physical occurrence of T_0 can be confirmed by in other measurable quantities, such as the average front velocity, see Fig. 6. The front speed is estimated by comparing consecutive measurements of the radius and using a finite-differences approach. The two panels show the same data, the only difference between them being that the bottom one is shown in logarithmic scale. We can see how the data divide into two sequences of points with slightly different scaling behavior, with the division approximately corresponding to $T_0 = 297$ h.

Coming back to the simulations of Eq. (2), Fig. 5(b) indicates a change in the scaling behavior of the global roughness at time $t_0 = 0.14$ [T], with a roughness of $w_0 = 0.044$ [L], where [L] and [T] are length and time units, respectively. Thus, the end of the experiment should correspond to a roughness $w_e = 0.044$ [L] $\times 1.9 = 0.084$ [L], which takes place at $t_e \sim 0.44$ [T]. We make this time correspond to $T_e = 801$ h. Thus, the numerical conversion from arbitrary time units to hours is 801 h/0.44 [T] $\approx$ 1800 h/[T]. The same reasoning can be performed with the length unit and we obtain a conversion factor of 0.47 mm/0.044 [L] $\approx$ 11 mm/[L]. Alternative procedures can be designed to obtain the conversion factors, and they all provide similar results. At any rate, using the indicated conversion factors we can estimate the physical values of the equation parameters in physical units, namely, $A_0 = 0$ mm/h, $A_1 = 0.067$ mm^2/h, $A_a = 6.1 \times 10^{-3}$ mm/h, $A_n = 0.086\,\mathrm{mm}^{3/2}/\mathrm{h}^{1/2}$. Experimental data are compared with simulations for this parameter choice in Fig. 7. With respect to $W(t)$, agreement is reached for essentially the full duration of the experiments. For times longer than approximately 800 h (which remain beyond our experimental setup), Eq. (2) predicts almost linear increase with time for $W(t)$ and $R(t)$. The agreement between experimental and simulation data is slightly worse in the case of $R(t)$, for which the initial condition

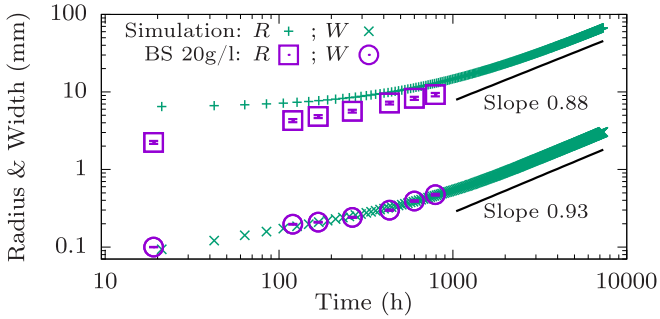

FIG. 7. Evolution of the radius and global roughness predicted by Eq. (2) with physical parameters $A_0 = 0$ mm/h, $A_1 = 0.067$ mm^2/h, $A_a = 6.1 \times 10^{-3}$ mm/h, $A_n = 0.086$ mm$^{3/2}$/h$^{1/2}$. Squares (circles) are experimental radius (roughness) for BS with $C_n = 20$ g/l; error bars are of the same size as symbols or smaller, see the Appendix.

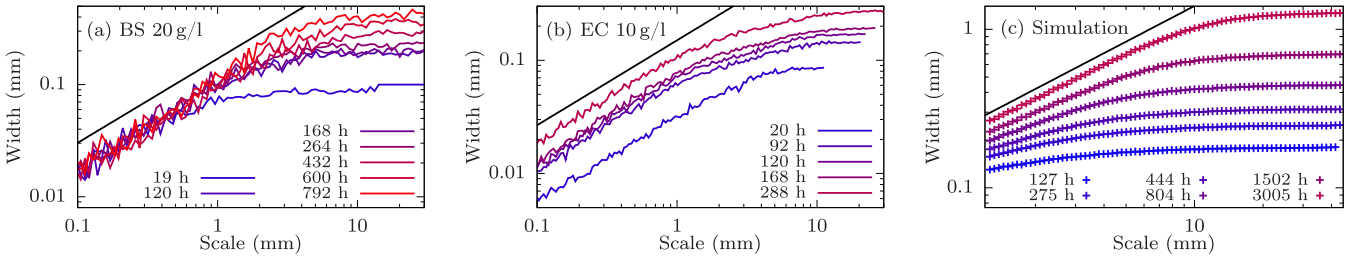

FIG. 8. Experimental length-scale dependence of the local roughness of BS (a) and EC (b) colony fronts for different times and C_n as indicated in the legends. (c) Same observable for numerical simulations of Eq. (2) as in Fig. 3. All straight lines represent $w(\ell) \sim \ell^{0.75}$.

plays a stronger role in the continuum model. Nevertheless, agreement also becomes quantitative for $t > 100$ h. Note, the time t_1 required for the onset of long-time, asymptotic behavior in the experiments can be assessed from the numerical simulation of Eq. (2), see the bottom panel of Fig. 5. We estimate $t_1 = 0.8$, which approximately corresponds to 1440 hours. Overall, Fig. 7 suggests that the scaling behavior reached in the experiments is preasymptotic, clear-cut asymptotics occurring for $t > t_1$, approximately twice our longest experimental growth time.

B. Geometrical properties: Local roughness and radial correlations

Further non-trivial properties of the experimental colonies involve the spatial dependence of front fluctuations. We can characterize them quantitatively by considering the so-called local roughness, $w(\ell)$, which evaluates interface deviations from an average position, within observation windows of size ℓ [9–11]. We proceed as is customary for systems with an overall circular symmetry [11,51]: Namely, each point on the front is converted to polar coordinates emanating from the geometric center, $(x_i, y_i) \to (\theta_i, r_i)$, whereby θ_i (r_i) is considered a new independent (dependent) variable. Given an initial point $\vec{r}_0$ and a length scale ℓ, we consider the set of points within a circle centered at $\vec{r}_0$ with radius ℓ. Then, we make a fit to the straight line which minimizes the deviations. The mean-square distance of the front positions to that fitting line provides the *local* roughness $w(\ell)$. Results for our experimental BS and EC colonies are displayed in Fig. 8. An approximate power-law dependence, $w(\ell) \sim \ell^{\alpha}$, holds at intermediate scales above 100 μm, and up to 3 mm for the most favorable cases, with $\alpha \simeq 0.75$. For the sake of comparison, we recall that a one-dimensional interface provided by the world-line of an uncorrelated random walk features $\alpha_{\rm RW} = 1/2$ [9–11]. Our experimental value for α is in the same range as those found earlier for similar bacterial colony experiments [8,13,14] and is also similar to values measured in other DL systems, like 1D ECD [54,55] or 2D thin films grown by CVD under low sticking conditions [46,56]. In these contexts, such large α are known not to correspond to any well-defined universality class of kinetic roughening [16,40,47], but to merely reflect the large surface slopes that ensue, due to diffusive instabilities. Such instabilities are actually well known to correlate with front branching [9–11], which in our experiments can be assessed through the behavior of the autocorrelation of the radial interface fluctuations as a function of the angular distance,

$$C(\Delta\theta, t) = \langle [r(\theta, t) - R(t)][r(\theta + \Delta\theta, t) - R(t)] \rangle. \quad (6)$$

As seen in Fig. 9, and in spite of the compactness of the colonies, $C(\Delta\theta, t)$ vanishes approximately at the same angular distance for different times, indicating fronts that develop well-defined branches. Moreover, the importance of such branching increases monotonically along the experimental time evolution. Such a behavior is analogous to the result of detailed continuum models of bacterial colony growth put forward in [35,36], which predict unconditional instability of the colony front to perturbations for a variety of relaxation mechanisms that include both, chemotactic and volumetric expansions. In application of the analysis in [35,36] to our data, Fig. 10 shows the time evolution of the area or perimeter ratio for the experimental colonies, compared to the $R(t)/2$ value that would correspond to a perfectly circular front in each case; clearly the actual perimeter grows too fast with time relative to the enclosed area, as compared with expectations for an ideally circular front. Such a behavior is inconsistent in particular with the occurrence of Eden behavior at long times [9–11].

The geometrical properties of the front observed in the experiments are very similarly found also in the simulations of Eq. (2). Figure 8 shows the dependence of the simulated local

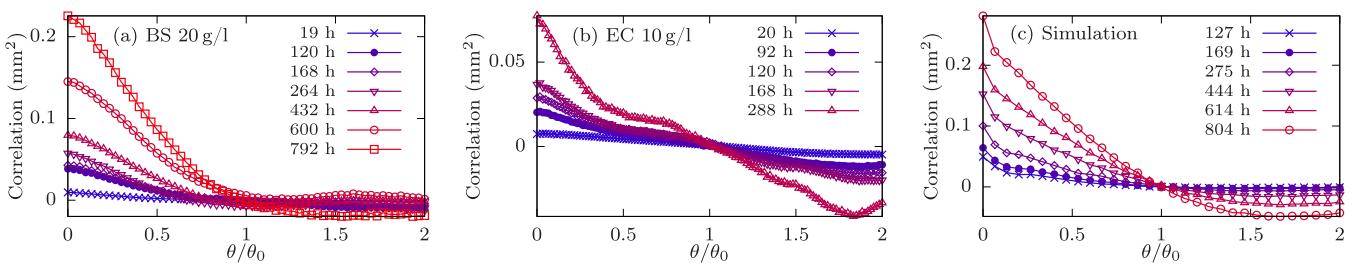

FIG. 9. Left to right: Autocorrelation function of experimental radial fluctuations vs angular distance rescaled by θ_0, for BS (a), EC (b), and simulations (c) of Eq. (2) with parameters as in Fig. 3, where $\theta_0 = 30°, 60°$, and $15°$, respectively. Times and C_n are as given in the legends.

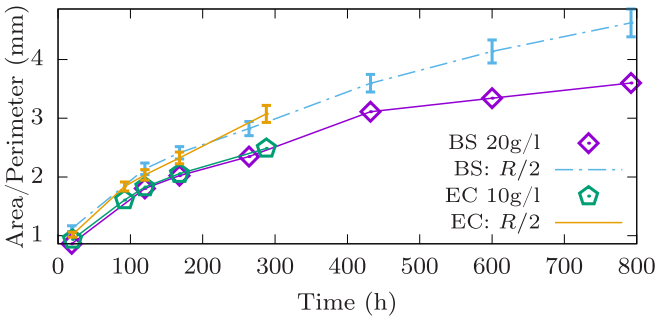

FIG. 10. Experimental area/perimeter ratio vs time. Symbols are direct measurements for conditions described in the legend; lines show $R(t)/2$ as obtained from Fig. 4 for the corresponding sets of data.

roughness with length scale for different times, readily compared with the experimental data in the same figure. Indeed, for small scales the model yields $w(\ell) \sim \ell^{\alpha}$, with α increasing with time up to 0.75, very close to the experimental value. Comparison between the model and the experiments improves with increasing times, as typical length-scales also increase. Note, these simulation data include the long-time, asymptotic regime identified for the model in Fig. 4. Finally, the behavior in simulations of the radial autocorrelation function $C(\Delta\theta,t)$ also supports our interpretation on branching at the interface: Fig. 9 indeed shows the selection of a precise correlation angle value θ_0, analogous to the experimental morphologies.

V. DISCUSSION AND CONCLUSIONS

Summarizing our experimental observations for both BS and EC colonies in the suppressed-motility conditions [14,15,39] which are in the classically alleged Eden regime, we obtain branched interfaces with scaling exponents $\beta \simeq 0.5$ and $\alpha \simeq 0.75$, which unambiguously differ from Eden-KPZ behavior, characterized by non-branched interfaces, $\beta_{\rm KPZ} = 1/3$, and $\alpha_{\rm KPZ} = 1/2$ [9–11]. Our experimental data are also inconsistent with quenched noise effects which, e.g., allegedly induce $\beta = 0.61, \alpha = 0.68$ in agent-based simulations of bacterial colonies [8], or with the so-called quenched KPZ (qKPZ) equation [10]. Unconditioned by any comparison to models, the fact that our experimental colony profiles become increasingly branched during all accessible times (Figs. 9 and 10) moreover suggests that the observed scaling is preasymptotic behavior for a system whose asymptotics is not Eden, and we speculate that this could also be the case for other, classical, experiments [13,14] performed under conditions which are similar to ours.

Given the semi-quantitative agreement between our experiments and simulations of the effective model, Eq. (2), we can consider the latter in order to predict what would be the actual asymptotic behavior of the former. Indeed, Eq. (2) predicts a long-time behavior with $\beta = 0.93$ (Fig. 4) and $\alpha = 0.75$ (Fig. 8). Actually, a small-slope approximation of Eq. (2) yields dimension-independent exponents $\alpha = \beta = 1$ [16,57]—recently measured in CVD under DL conditions [47]—which are definitely non-KPZ and are expected to characterize Eq. (2) at long times. Note, for interfaces with $\alpha \gtrsim 1$, local measurements using $w(\ell)$ are known to underestimate the correct value of the roughness exponent [40], explaining our $\alpha = 0.75$ value. Parameter conditions in our experiments would make such a long-time regime hardly accessible, requiring growth times at least twice the longest time that we have been able to reach, as estimated in Sec. IV A 1. On the other hand, the preasymptotic ($t < 800$ h) behavior in Eq. (2)—during which $W(t)$ evolves as in our experiments—is dominated by the diffusive (shadowing) instabilities that induce branching of the front and large exponent values. In such a case, and as shown for other DL systems [16,40,47], the exponent values are nonuniversal and may depend on parameter values and even on the specific space/time ranges in which power-law fits are attempted.

In conclusion, bacterial colonies where individual motility is suppressed form compact aggregates whose front morphology can still be dominated by diffusive instabilities. For our experimental conditions, similar to those in [14,15,39], preasymptotic scaling seems to occur at the accessed times, which in any case is not in the Eden-KPZ universality class. There is no need to invoke quenched disorder to account for this discrepancy. Rather, the shadowing instability induces large front fluctuations with non-universal scaling. This behavior is strongly reminiscent of many other experimental systems [41,46,54–56] in which transport-induced instabilities induce effective scaling. In some of these cases [41] the observed kinetic roughening properties have also been associated with the qKPZ universality class, due to accidental similarities in the values of the scaling exponents [42–44]. Note, attributing a set of scaling exponents to a well-defined, asymptotic, universality class like qKPZ, or to nonuniversal preasymptotic behavior as we are presently advocating for, are conceptually very different interpretations.

Non-KPZ exponents due to diffusive instabilities are also predicted by agent-based simulations [37,38] for small values of the active layer thickness δ. However, for sufficiently large δ very compact colonies with extremely flat fronts are found [37,38]. While this seemingly questions the prevalence of diffusive instabilities, continuum models [35,36] analytically predict such flat front conditions to be a finite-size effect. Thus, parameter conditions select a typical length-scale ℓ_0 for the instabilities, which is well defined for any value of δ. As standard in pattern formation [58], the correlation length along the front (initially a few cell sizes across) needs to increase up to ℓ_0 for the instability to set in. If ℓ_0 is very large (in band geometry, for systems smaller than ℓ_0), the front may effectively be flat. In circular geometries, for sufficiently (perhaps, exceedingly) long times, the instability will still occur.

We should still note that additional systems exist, which are closely related to the ones we study, and for which Eden-KPZ scaling does occur. For instance, bacterial colonies for which individual motility is non-negligible [14] yield a roughness exponent compatible with the 1D KPZ value. Also, aggregates of non-cancerous (Vero) or cancerous (HeLa) primate cells display unambiguous KPZ [53], and even qKPZ [59,60], scaling, as is the case with fungal growth [61]. Experimentally, KPZ scaling also applies to fluctuating frontiers between different genetic strains in range expansion of *E. coli* [62], although deviations from Eden behavior can also occur [63,64]. In general, individual cell motility seems to play a relevant

role, to the extent that instabilities associated with nutrient transport can eventually be superseded. Indeed, the Eden model [22] will at any rate stand as the prime example for reaction-limited growth [9–11], where nutrient transport is, effectively, infinitely fast and irrelevant to front fluctuations.

ACKNOWLEDGMENTS

We acknowledge fruitful conversations with G. Melaugh and K. A. Takeuchi. This work has been supported by Ministerio de Economía y Competitividad, Agencia Estatal de Investigación, and Fondo Europeo de Desarrollo Regional (Spain and European Union) through Grants No. FIS2015-66020-C2-1-P, FIS2015-69167-C2-1-P, FIS2015-73337-JIN, and BIO2016-79618-R, and by Comunidad Autónoma de Madrid (Spain) Grant No. NANOAVANSENS S2013/MIT-3029.

APPENDIX: SOME ERROR ESTIMATES

For each bacterial species and nutrient concentration we have only one sample available. Therefore, the error bars on the measurements of the radius and the roughness cannot be estimated via statistical error between different samples. An alternative approach is to consider that measurements performed on different parts of the interface constitute a suitable statistical ensemble from which we can estimate the magnitude of the desired fluctuations. Thus, the global roughness itself provides an estimate for the uncertainty in the measurement of the radius.

The estimate of the fluctuations of the roughness is more involved. Our approach is to divide the interface into patches of size ℓ and measure the estimate for each of them, $W_i(\ell)$.

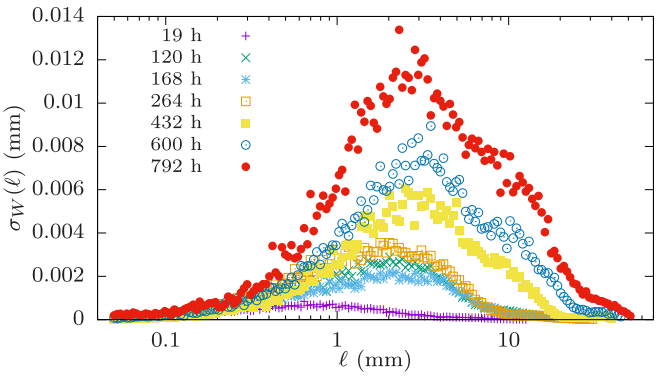

FIG. 11. Scale dependence of the estimate for the error in the global roughness obtained using Eq. (A1), when applied to the profiles of our BS sample grown with $C_n = 20$ g/l. The actual estimate is provided by the maximum of each curve.

Then, for each size ℓ we can determine the deviation of those measures,

$$\sigma_W^2(\ell) = \langle W^2(\ell)\rangle - \langle W(\ell)\rangle^2. \tag{A1}$$

Naturally, this deviation will depend on the measurement scale ℓ. We have thus chosen the worst case to determine our estimate for the error in the roughness, namely,

$$\sigma_W^2 = \max_\ell \sigma_W^2(\ell). \tag{A2}$$

This is how the error bars are estimated in Fig. 7. The behavior of $\sigma_W(\ell)$ for the fronts of BS colonies grown with $C_n = 20$ g/l is shown as an illustration in Fig. 11.

[1] S. Ramaswamy, Annu. Rev. Condens. Matter Phys. **1**, 323 (2010).
[2] M. C. Marchetti, J. F. Joanny, S. Ramaswamy, T. B. Liverpool, J. Prost, M. Rao, and R. A. Simha, Rev. Mod. Phys. **85**, 1143 (2013).
[3] E. Ben-Jacob, I. Cohen, and H. Levine, Adv. Phys. **49**, 395 (2000).
[4] A. Sokolov, I. S. Aranson, J. O. Kessler, and R. E. Goldstein, Phys. Rev. Lett. **98**, 158102 (2007).
[5] H. P. Zhang, A. Be'er, E.-L. Florin, and H. L. Swinney, Proc. Natl. Acad. Sci. U.S.A. **107**, 13626 (2010).
[6] E. Ben-Jacob, I. Cohen, and D. L. Gutnick, Annu. Rev. Microbiol. **52**, 779 (1998).
[7] M. Matsushita, F. Hiramatsu, N. Kobayashi, T. Ozawa, Y. Yamazaki, and T. Matsuyama, Biofilms **1**, 305 (2004).
[8] J. A. Bonachela, C. D. Nadell, J. B. Xavier, and S. A. Levin, J. Stat. Phys. **144**, 303 (2011).
[9] T. Vicsek, *Fractal Growth Phenomena* (World Scientific, Singapore, 1992).
[10] A.-L. Barabási and H. E. Stanley, *Fractal Concepts in Surface Growth* (Cambridge University Press, New York, 1995).
[11] P. Meakin, *Fractals, Scaling and Growth far from Equilibrium* (Cambridge University Press, Cambridge, 1998).
[12] H. Fujikawa and M. Matsushita, J. Phys. Soc. Jpn. **58**, 3875 (1989).
[13] T. Vicsek, M. Cserzö, and V. K. Horváth, Physica A **167**, 315 (1990).
[14] J. I. Wakita, H. Itoh, T. Matsuyama, and M. Matsushita, J. Phys. Soc. Jpn. **66**, 67 (1997).
[15] M. Matsushita, J. Wakita, H. Itoh, I. Ràfols, T. Matsuyama, H. Sakaguchi, and M. Mimura, Physica A **249**, 517 (1998).
[16] M. Nicoli, M. Castro, and R. Cuerno, J. Stat. Mech.: Theory Exp. (2009) P02036.
[17] C. D. Nadell, K. R. Foster, and J. B. Xavier, PLoS Comp. Biol. **6**, e1000716 (2010).
[18] S. Mitri, J. B. Xavier, and K. R. Foster, Proc. Natl. Acad. Sci. U.S.A. **108**, 10839 (2011).
[19] C. D. Nadell, V. Bucci, K. Drescher, S. A. Levin, B. L. Bassler, and J. B. Xavier, Proc. R. Soc. London B **280**, 20122770 (2013).
[20] J. W. Costerton, Z. Lewandowski, D. E. Caldwell, D. R. Korber, and H. M. Lappin-Scott, Annu. Rev. Microbiol. **49**, 711 (1995).
[21] J. N. Wilking, T. E. Angelini, A. Seminara, M. P. Brenner, and D. A. Weitz, MRS Bull. **36**, 385 (2011).
[22] M. Eden, in *Proceedings of the 4th Berkeley Symposium on Mathematical Statistics and Probability*, Vol. 4, edited by J. Neyman (University of California Press, Berkeley, 1961), pp. 223–239.

[23] M. Kardar, G. Parisi, and Y.-C. Zhang, Phys. Rev. Lett. **56**, 889 (1986).
[24] S. G. Alves, T. J. Oliveira, and S. C. Ferreira, Europhys. Lett. **96**, 48003 (2011).
[25] K. A. Takeuchi, J. Stat. Mech.: Theory Exp. (2012) P05007.
[26] T. Halpin-Healy and K. A. Takeuchi, J. Stat. Phys. **160**, 794 (2015).
[27] H. Van Beijeren, Phys. Rev. Lett. **108**, 180601 (2012).
[28] C. B. Mendl and H. Spohn, Phys. Rev. Lett. **111**, 230601 (2013).
[29] M. Kulkarni and A. Lamacraft, Phys. Rev. A **88**, 021603(R) (2013).
[30] S. Nesic, R. Cuerno, and E. Moro, Phys. Rev. Lett. **113**, 180602 (2014).
[31] A. M. Lacasta, I. R. Cantalapiedra, C. E. Auguet, A. Peñaranda, and L. Ramírez-Piscina, Phys. Rev. E **59**, 7036 (1999).
[32] M. Mimura, H. Sakaguchi, and M. Matsushita, Physica A **282**, 283 (2000).
[33] J. Dockery and I. Klapper, SIAM J. Appl. Math. **62**, 853 (2002).
[34] N. Kobayashi, O. Moriyama, S. Kitsunezaki, Y. Yamazaki, and M. Matsushita, J. Phys. Soc. Jpn. **73**, 2112 (2004).
[35] C. Giverso, M. Verani, and P. Ciarletta, J. R. Soc., Interface **12**, 20141290 (2015).
[36] C. Giverso, M. Verani, and P. Ciarletta, Biomech. Model. Mechanobiol. **15**, 643 (2016).
[37] F. D. C. Farrell, O. Hallatschek, D. Marenduzzo, and B. Waclaw, Phys. Rev. Lett. **111**, 168101 (2013).
[38] F. D. Farrell, M. Gralka, O. Hallatschek, and B. Waclaw, J. R. Soc., Interface **14**, 20170073 (2017).
[39] I. Ràfols, Formation of concentric rings in bacterial colonies, Master's thesis, Chuo University, 1998.
[40] M. Castro, R. Cuerno, A. Sánchez, and F. Domínguez-Adame, Phys. Rev. E **62**, 161 (2000).
[41] P. J. Yunker, M. A. Lohr, T. Still, A. Borodin, D. J. Durian, and A. G. Yodh, Phys. Rev. Lett. **110**, 035501 (2013).
[42] M. Nicoli, R. Cuerno, and M. Castro, Phys. Rev. Lett. **111**, 209601 (2013).
[43] P. J. Yunker, M. A. Lohr, T. Still, A. Borodin, D. J. Durian, and A. G. Yodh, Phys. Rev. Lett. **111**, 209602 (2013).
[44] T. J. Oliveira and F. D. A. Aarão Reis, J. Stat. Mech.: Theory Exp. (2014) P09006.
[45] G. S. Bales, R. Bruinsma, E. A. Eklund, R. P. U. Karunasiri, J. Rudnick, and A. Zangwill, Science **249**, 264 (1990).
[46] F. Ojeda, R. Cuerno, R. Salvarezza, and L. Vázquez, Phys. Rev. Lett. **84**, 3125 (2000).
[47] M. Castro, R. Cuerno, M. Nicoli, L. Vázquez, and J. G. Buijnsters, New J. Phys. **14**, 103039 (2012).
[48] M. L. Frankel and G. I. Sivashinsky, Phys. Rev. E **52**, 6154 (1995).
[49] S. I. Blinnikov and P. V. Sasorov, Phys. Rev. E **53**, 4827 (1996).
[50] J. Rodríguez-Laguna, S. N. Santalla, and R. Cuerno, J. Stat. Mech.: Theory Exp. (2011) P05032.
[51] S. N. Santalla, J. Rodríguez-Laguna, and R. Cuerno, Phys. Rev. E **89**, 010401(R) (2014).
[52] K. A. Takeuchi and M. Sano, Phys. Rev. Lett. **104**, 230601 (2010).
[53] M. A. C. Huergo, M. Pasquale, P. H. González, A. E. Bolzán, and A. J. Arvia, Phys. Rev. E **84**, 021917 (2011).
[54] J. M. Pastor and M. A. Rubio, Phys. Rev. Lett. **76**, 1848 (1996).
[55] S. Huo and W. Schwarzacher, Phys. Rev. Lett. **86**, 256 (2001).
[56] Y. P. Zhao, J. B. Fortin, G. Bonvallet, G. C. Wang, and T. M. Lu, Phys. Rev. Lett. **85**, 3229 (2000).
[57] M. Nicoli, R. Cuerno, and M. Castro, Phys. Rev. Lett. **102**, 256102 (2009).
[58] M. Cross and H. Greenside, *Pattern Formation and Dynamics in Nonequilibrium Systems* (Cambridge University Press, Cambridge, 2009).
[59] M. A. C. Huergo, N. E. Muzzio, M. A. Pasquale, P. H. Pedro González, A. E. Bolzán, and A. J. Arvia, Phys. Rev. E **90**, 022706 (2014).
[60] N. E. Muzzio, M. A. Pasquale, M. A. C. Huergo, A. E. Bolzán, P. H. González, and A. J. Arvia, J. Biol. Phys. **42**, 477 (2016).
[61] J. M. López and H. J. Jensen, Phys. Rev. E **65**, 021903 (2002).
[62] O. Hallatschek, P. Hersen, S. Ramanathan, and D. R. Nelson, Proc. Natl. Acad. Sci. U.S.A. **104**, 19926 (2007).
[63] J. T. Kuhr, M. Leisner, and E. Frey, New J. Phys. **13**, 113013 (2011).
[64] M. Reiter, S. Rulands, and E. Frey, Phys. Rev. Lett. **112**, 148103 (2014).